Diffraction at ALICE

Rainer Schicker[1],

[1]Physikalisches Institut, Philosophenweg 12, 69120 Heidelberg, Germany

The ALICE detector at the Large Hadron Collider (LHC) consists of a central barrel, a muon spectrometer, zero degree calorimeters and additional detectors which are used for trigger purposes and for event classification. The performance of the ALICE central barrel is discussed. The trigger strategy for diffractive events is outlined. The physics potential of studying diffractive processes at the LHC is presented by investigating observables of the Pomeron and Odderon. Possible signatures of gluon saturation in diffractive events are discussed.

1 The ALICE Experiment

The ALICE experiment is presently being built and commissioned at the Large Hadron Collider (LHC) [1, 2]. The ALICE experiment consists of a central barrel covering the pseudorapidity range $-0.9 < \eta < 0.9$ and a muon spectrometer in the range $-4.0 < \eta < -2.4$. Additional detectors for trigger purposes and for event classification exist such that the range $-4.0 < \eta < 5.0$ is covered. The ALICE physics program foresees data taking in pp and PbPb collisions at luminosities up to $\mathcal{L} = \bigtriangledown \times 10^{30}\mathrm{cm}^{-2}\mathrm{s}^{-1}$ and $\mathcal{L} = 10^{27}\mathrm{cm}^{-2}\mathrm{s}^{-1}$, respectively. An asymmetric system pPb will be measured at a luminosity of $\mathcal{L} = 10^{29}\mathrm{cm}^{-2}\mathrm{s}^{-1}$.

2 The ALICE Central Barrel

The detectors in the ALICE central barrel track and identify hadrons, electrons and photons in the pseudorapidity range $-0.9 < \eta < 0.9$. The magnetic field strength of 0.5 T allows the measurement of tracks from very low transverse momenta of about $100\,\mathrm{MeV}/c$ to fairly high values of about 100 GeV/c. The tracking detectors are designed to reconstruct secondary vertices from decays of hyperons, D and B mesons. The granularity of the central barrel detectors is chosen such that particle tracking and identification can be achieved in a high multiplicity environment of up to 8000 particles per unit of rapidity. The main detector systems for these tasks are the Inner Tracking System (ITS), the Time Projection Chamber (TPC), the Transition Radiation Detector (TRD) and the Time of Flight array (TOF). These systems cover the full azimuthal angle within the pseudorapidity range $-0.9 < \eta < 0.9$. Additional detectors with partial coverage of the central barrel are a PHOton Spectrometer (PHOS), an electromagnetic calorimeter (EMCAL) and a High-Momentum Particle Identification Detector (HMPID).

2.1 The Central Barrel Performance

The ITS, TPC and TRD detectors are the main tracking detectors in the central barrel. With the information from these detectors, pions with momenta as low as 100 MeV/c can be tracked. The combined transverse momentum resolution from the ITS, TPC and TRD detector is expected to be about 3% at a transverse momentum of $p_T = 100\,\mathrm{GeV}/c$.

Particle identification is achieved in the central barrel by different methods. The specific energy loss is measured by the TPC, the TRD and the strip and drift detectors of the ITS.

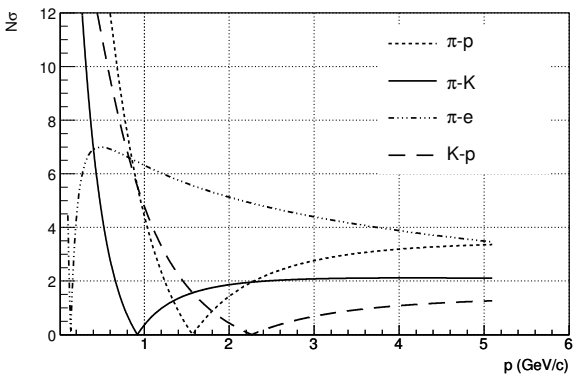

Figure 1: Particle identification by dE/dx measurement.

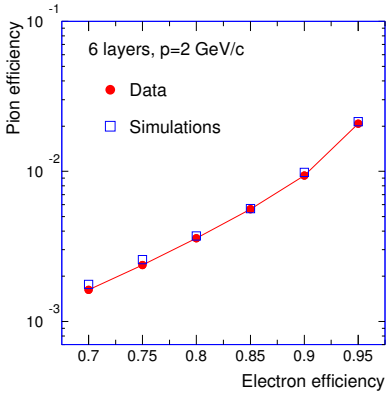

Figure 2: Electron-pion separation in the TRD.

Fig. 1 shows the separation power of the TPC as a function of momentum. The separation of pairs of different particle species is shown in units of the resolution of the dE/dx measurement.

The electron-pion separation at high momenta is significantly improved by the information of the TRD system. Fig. 2 shows the pion efficiency in the TRD as a function of the electron efficiency. Here, pion efficiency indicates that a pion is misidentified as an electron. The expected TRD performance for a full stack of six layers is shown by the squares and compared to test beam data represented by the circles.

3 The ALICE Zero Degree Neutron Calorimeter

The Zero Degree Neutron Calorimeters (ZDC) are placed on both sides of the interaction point at a distance of 116 m [3]. The ZDC information can be used to select different diffractive topologies. Events of the type $pp \rightarrow ppX$ do not deposit energy in these calorimeters, single diffractive dissociation events $pp \rightarrow pp^*X$ will have energy in one of the calorimeters whereas double diffractive dissociation events $pp \rightarrow p^*p^*X$ will have energy deposited in both calorimeters. Here, p^* denotes a diffractively excited state of the proton and X represents a centrally produced diffractive state from which the diffractive L0 trigger is derived as described below.

4 The ALICE Diffractive Gap Trigger

Additional detectors for event classification and trigger purposes are located on both sides of the ALICE central barrel. First, two arrays of scintillator detectors V0A and V0C cover a

pseudorapidity interval of about two units on either side of the central barrel with a fourfold segmentation of half a unit. The azimuthal coverage is divided into eight segments of 45 degrees hence each array is composed of 32 individual counters. Second, a Forward Multiplicity Detector (FMD) is located on both sides of the central barrel. The pseudorapidity coverage of this detector is $-3.4 < \eta < -1.7$ and $1.7 < \eta < 5.1$, respectively.

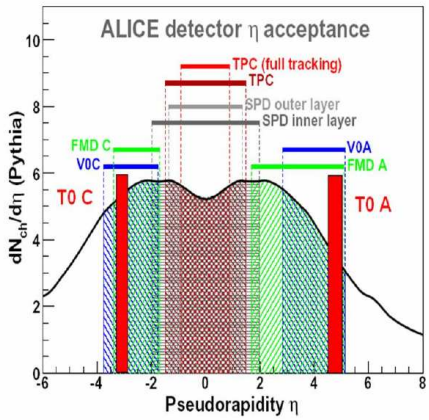

Figure 3: Pseudorapidity coverage of trigger detectors and of detectors in central barrel.

Fig. 3 shows the pseudorapidity coverage of the detector systems described above. The geometry of the ALICE central barrel in conjunction with the additional detectors V0A,V0C and FMD is well suited for the definition of a rapidity gap trigger. The ALICE trigger system is designed as a multi-level scheme with L0, L1 and L2 levels and a High-Level Trigger (HLT). The L0 signal can be taken from the TOF detector or from the pixel detector of the ITS [4].

The HLT has access to the information of all the detectors shown in Fig. 3 and will hence be able to select events with rapidity gaps in the range $-4 < \eta < -1$ and $1 < \eta < 5$. These gaps extend over seven units of pseudorapidity and are hence expected to suppress minimum bias inelastic events by many orders of magnitude.

5 ALICE Diffractive Physics

The tracking capabilities at very low transverse momenta in conjunction with the excellent particle identification make ALICE an unique facility at LHC to pursue a long term physics program of diffractive physics. The low luminosity of ALICE as compared to the other LHC experiments restricts the ALICE physics program to reactions with cross section at a level of a few nb per unit of rapidity.

Fig. 4 shows the transverse momentum acceptance of the four main LHC experiments. Not shown in this figure is the acceptance of the TOTEM experiment which has a physics program of measurements of total cross section, elastic scattering and soft diffraction [5]. The acceptance of the TOTEM telescopes is in the range of $3.1 < |\eta| < 4.7$ and $5.3 < |\eta| < 6.5$. The combined data taking of TOTEM and CMS represents the largest rapidity interval covered at the LHC. The CMS transverse momentum acceptance of about $1\,\mathrm{GeV}/c$ shown in Fig. 4 represents a

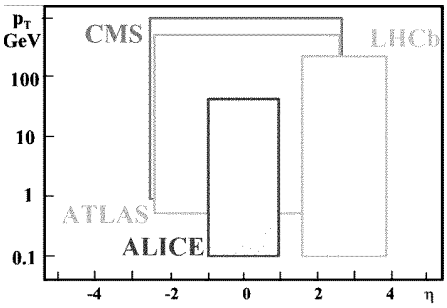

Figure 4: Rapidity and transverse momentum acceptance of the LHC experiments.

nominal value. The CMS analysis framework foresees the reconstruction of a few selected data samples to values as low as $0.2\,\mathrm{GeV}/c$ [6].

6 Signatures of the Pomeron

The geometry of the ALICE experiment is suited for measuring a centrally produced diffractive state with a rapidity gap on either side. Such a topology can result, among other, from double Pomeron exchange with subsequent hadronization of the central state. It is expected that the secondaries from Pomeron-Pomeron fusion events show markedly different characteristics as compared to secondaries from inelastic minimum bias events.

First, it is expected that the production cross section of glueball states in Pomeron fusion is larger as compared to inelastic minimum bias events. It will therefore be interesting to study the resonances produced in the central region when two rapidity gaps are required [7].

Second, the slope α' of the Pomeron trajectory is rather small: An analysis of proton-proton, proton-antiproton and photon-proton cross sections and of the proton structure function F_2 derives $\alpha' \sim 0.25\,\mathrm{GeV}^{-2}$ whereas a value $\alpha' \sim 0.1\,\mathrm{GeV}^{-2}$ is found in J/Ψ photoproduction at HERA [8]. These values of α' in conjunction with the small t-slope ($< 1\,\mathrm{GeV}^{-2}$) of the triple Pomeron vertex indicate that the mean transverse momentum k_t in the Pomeron wave function is relatively large $\alpha' \sim 1/k_t^2$, most probably $k_t > 1\,\mathrm{GeV}$. The transverse momenta of secondaries produced in Pomeron-Pomeron interactions are of the order of this k_t. Thus the mean transverse momenta of secondaries produced in Pomeron-Pomeron fusion is expected to be larger as compared to inelastic minimum bias events.

Third, the large k_t described above corresponds to a large effective temperature. A suppression of strange quark production is not expected. Hence the K/π ratio is expected to be enhanced in Pomeron-Pomeron fusion as compared to inelastic minimum bias events [9]. Similarly, the η/π and η'/π ratios are expected to be enhanced due to the hidden strangeness content and due to the gluon components in the Fock states of η, η'.

7 Signatures of the Odderon

The Odderon was first postulated in 1973 and is represented by color-singlet exchange with negative C-parity [10]. Finding experimental evidence of the Odderon has, however, turned out to be extremely difficult [11].

7.1 Signatures of Odderon Cross Sections

Signatures of Odderon exchanges can be looked for in exclusive reactions where the Odderon (besides the photon) is the only possible exchange. Diffractively produced C-odd states such as vector mesons $\phi, J/\psi, \Upsilon$ can result from photon-Pomeron or Odderon-Pomeron exchange. Any excess beyond the photon contribution would be indication of an Odderon exchange.

Fig. 5 and Fig. 6 show the Feynman diagram for vector meson production by Pomeron-Odderon fusion with the protons staying intact and with breakup, respectively. The two different reaction channels can be identified by the information of the ZDC. To each of these two diagrams exists a diagram in which the Odderon is replaced by a photon.

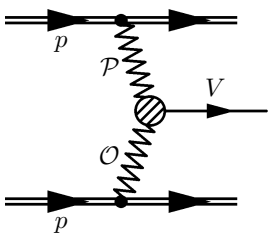

Figure 5: Vector Meson production by Odderon-Pomeron fusion without proton breakup.

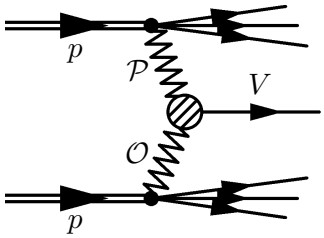

Figure 6: Vector Meson production by Odderon-Pomeron fusion with proton breakup.

Cross sections for diffractively produced J/ψ in pp collisions at LHC energies were first estimated by Schäfer et al. [12]. Calculations by Bzdak et al result in t-integrated photon and Odderon contributions of $\frac{d\sigma}{dy}\,|_{y=0} \sim 15\,\text{nb}$ and $\frac{d\sigma}{dy}\,|_{y=0} \sim 1\,\text{nb}$, respectively [13].

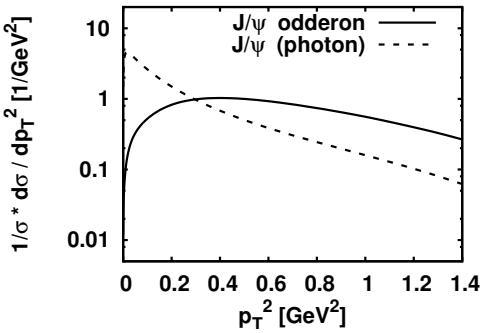

Figure 7: The J/ψ transverse momentum distribution for the photon and Odderon contributions.

The calculated cross sections for the Odderon and photon contribution carry large uncertainties, the upper and lower limit vary by about an order of magnitude. This cross section is, however, at a level where in 10^6 s of data taking the J/ψ can be measured in its e^+e^- decay

channel at a level of 4% statistical uncertainty. Due to the different t-dependence, the two contributions result in different p_T distributions of the J/ψ. The photon and Odderon contributions are shown in Fig. 7 by the dotted and solid lines, respectively [14]. A careful analysis of the J/ψ transverse momentum might therefore allow to disentangle the Odderon contribution.

7.2 Signatures of Odderon Interference Effects

If the diffractively produced final state is not an eigenstate of C-parity, then interference effects between photon-Pomeron and photon-Odderon amplitudes can be analysed.

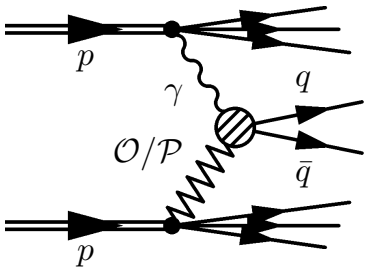

Figure 8: photon-Pomeron and photon-Odderon amplitudes.

Fig. 8 shows the photon-Pomeron and the photon-Odderon amplitudes for $q\bar{q}$ production.

A study of open charm diffractive photoproduction estimates the asymmetry in fractional energy to be on the order of 15% [15]. The forward-backward charge asymmetry in diffractive production of pion pairs is calculated to be on the order of 10% for pair masses in the range $1\,\mathrm{GeV}/c^2 < m_{\pi+\pi-} < 1.3\,\mathrm{GeV}/c^2$ [16, 17].

8 Photoproduction of heavy quarks

Diffractive reactions involve scattering on small-x gluons in the proton. The number density of gluons at given x increases with Q^2, as described by the DGLAP evolution. Here, Q^2 and x denote the kinematic parameters used in deep inelastice ep scattering. The transverse gluon density at a given Q^2 increases with decreasing x as described by the BFKL evolution equation. At some density, gluons will overlap and hence reinteract. In this regime, the gluon density saturates and the linear DGLAP and BFKL equation reach their range of applicability. A saturation scale $Q_s(x)$ is defined which represents the breakdown of the linear regime. Nonlinear effects become visible for $Q < Q_s(x)$.

Diffractive heavy quark photoproduction represents an interesting probe to look for gluon saturation effects at LHC. The inclusive cross section for $Q\bar{Q}$ photoproduction can be calculated within the dipole formalism. In this approach, the photon fluctuates into a $Q\bar{Q}$ excitation which interacts with the proton as a color dipole. The dipole cross section $\sigma(x, r)$ depends on x as well as on the transverse distance r of the $Q\bar{Q}$ pair. A study of inclusive heavy quark photoproduction in pp collisions at LHC energy has been carried out [18]. These studies arrive

at differential cross sections for open charm photoproduction of $\frac{d\sigma}{dy}\mid_{y=0} \sim 1.3\,\mu$b within the collinear pQCD approach as compared to $\frac{d\sigma}{dy}\mid_{y=0} \sim 0.4\,\mu$b within the colour glass condensate (CGC). The cross sections are such that open charm photoproduction seems measurable with good statistical significance. The corresponding numbers for the cross section for bottom photoproduction are $\frac{d\sigma}{dy}\mid_{y=0} \sim 20\,$nb and 10 nb, respectively.

Diffractive photoproduction is characterized by two rapidity gaps in the final state. In the dipole formalism described above, the two gluons of the color dipole interaction are in color singlet state. Diffractive heavy quark photoproduction cross sections in pp, pPb and PbPb collisions at LHC have been studied [19]. The cross sections for diffractive charm photoproduction are $\frac{d\sigma}{dy}\mid_{y=0} \sim 6\,$nb in pp, $\frac{d\sigma}{dy}\mid_{y=0} \sim 9\,\mu$b in pPb and $\frac{d\sigma}{dy}\mid_{y=0} \sim 11\,$mb in PbPb collisions. The corresponding numbers for diffractive bottom photoproduction are $\frac{d\sigma}{dy}\mid_{y=0} \sim 0.014\,$nb in pp, $\frac{d\sigma}{dy}\mid_{y=0} \sim 0.016\,\mu$b in pPb and $\frac{d\sigma}{dy}\mid_{y=0} \sim 0.02\,$mb in PbPb collisions.

Heavy quarks with two rapidity gaps in the final state can, however, also be produced by central exclusive production, i.e. two Pomeron fusion. The two production mechanisms have a different t-dependence. A careful analysis of the transverse momentum p_T of the $Q\bar{Q}$ pair might therefore allow to disentangle the two contributions.

Acknowledgements

I thank Otto Nachtmann and Carlo Ewerz for illuminating discussions and Leszek Motyka for preparing and communicating Figure 7.

This work is supported in part by German BMBF under project 06HD197D and by WP8 of the hadron physics program of the 7^{th} EU program period.

References

[1] F. Carminati et al, ALICE Collaboration, 2004, J.Phys. G: Nucl. Part. Phys. **30** 1517

[2] B. Alessandro et al, ALICE Collaboration, 2006, J.Phys. G: Nucl. Part. Phys. **32** 1295

[3] R. Arnaldi et al, Nucl. Instr. and Meth. A **564** (2006) 235

[4] The ALICE collaboration, K. Aamodt et al, The ALICE experiment at the CERN LHC, (2008) JINST_3_S08002

[5] S. Giani, Diffraction at TOTEM, these proceedings

[6] D. d'Enterria et al, Addendum CMS technical design report, J. Phys. G34:2307-2455, 2007

[7] F. Close, A. Kirk, G. Schuler, Phys.Lett. B **477** (2000) 13

[8] A. Donnachie, P. Landshoff, Phys.Lett. B**595** (2004) 393

[9] T. Åkesson et al, Nucl. Phys. B **264** (1986) 154

[10] L. Lukaszuk, B. Nicolescu, Lett. Nuovo Cim. **8** (1973) 406

[11] C. Ewerz, Proceedings XII Rencontres de Blois (2005) 377

[12] A. Schäfer, L. Mankiewicz, O. Nachtmann, Phys.Lett. B **272** (1991) 419

[13] A. Bzdak, L. Motyka, L. Szymanowski, J.R. Cudell, Phys.Rev. D **75** (2007) 094023

[14] L. Motyka, private communication

[15] S.J. Brodsky, J. Rathsman, C. Merino, Phys.Lett. B **461** (1999) 114

[16] P. Hägler, B. Pire, L. Szymanowski, O.V. Teryaev, Phys.Lett. B **535** (2002) 117

[17] I.F. Ginzburg, I.P. Ivanov, N.N. Nikolaev, Eur.Phys.J. C**5** (2003) 02

[18] V.P. Goncalves, M.V. Machado, Phys.Rev.D **71** (2005) 014025

[19] V.P. Goncalves, M.V. Machado, Phys.Rev.D **75** (2007) 031502